

## **Supporting Information for**

### **Electrogenerated Chemiluminescence Logic Gate Operations Based on Molecule-responsive Organic Microwires**

Jianmin Gu,<sup>\*,[a]</sup> Jingxiao Wu,<sup>[a]</sup> Yahui Gao,<sup>[a]</sup> Tianhui Wu,<sup>[a]</sup> Qing  
Li,<sup>[c]</sup> Aixue Li,<sup>[a]</sup> Jian-Yao Zheng,<sup>[d]</sup> Bin Wen,<sup>\*,[b]</sup> and Faming Gao<sup>\*,[a]</sup>

E-mail: [jmgu@ysu.edu.cn](mailto:jmgu@ysu.edu.cn); [wenbin@ysu.edu.cn](mailto:wenbin@ysu.edu.cn); [fmgao@ysu.edu.cn](mailto:fmgao@ysu.edu.cn)

## Contents

- i. **Figure S1.** Molecular structure of 9,10-bis(phenylethynyl)anthracene (BPEA).
- ii. **Figure S2.** The bright-field microscopy image of the BPEA MWs.
- iii. **Figure S3.** The photograph of a typical ECL cell.
- iv. **Figure S4.** The cyclic voltammograms of BPEA MWs/ITO in 0.1 M KCl aqueous solution. Scan rate: 300 mV/s.
- v. **Figure S5.** Linear calibration plot for the dependence at wide DA concentration of BPEA MWs/ITO ECL system. K is the slope of the line; R is the Pearson product-moment correlation coefficient. Inset: Dependence of the ECL intensity of the BPEA MWs/ITO on the concentration of DA from a to g:  $1.0 \times 10^{-10}$  M,  $1.0 \times 10^{-9}$  M,  $1.0 \times 10^{-8}$  M,  $1.0 \times 10^{-7}$  M,  $1.0 \times 10^{-6}$  M,  $1.0 \times 10^{-5}$  M,  $1.0 \times 10^{-4}$  M. Scan rate: 300 mV/s.
- vi. **Figure S6.** Linear calibration plot for the dependence at wide Pro concentration of BPEA MWs/ITO ECL system. K is the slope of the line; R is the Pearson product-moment correlation coefficient. Inset: Dependence of the ECL intensity of the BPEA MWs/ITO on the concentration of Pro from a to f:  $1.0 \times 10^{-10}$  M,  $1.0 \times 10^{-8}$  M,  $1.0 \times 10^{-7}$  M,  $1.0 \times 10^{-6}$  M,  $1.0 \times 10^{-5}$  M,  $1.0 \times 10^{-3}$  M. Scan rate: 300 mV/s.
- vii. **Figure S7.** ECL emission signal of the BPEA MWs/ITO in 0.1 M KCl aqueous solution containing  $1.0 \times 10^{-5}$  M MB.
- viii. **Figure S8.** Spectral overlap between the PL emission spectrum of BPEA MWs (Black curve) and the absorption spectrum of MB dissolved in H<sub>2</sub>O (Red curve).
- ix. **Figure S9.** ECL kinetic curves of the OR logic gate.
- x. **Figure S10.** ECL kinetic curves of the XOR logic gate.
- xi. **Figure S11.** ECL kinetic curves of the INHIBIT logic gate.
- xii. **Figure S12.** Schematic representation of the ECL system which performs the (a) OR, (b) XOR and (c) INHIBIT logic gates under the

presence of other concentrations of ECL active molecules. The bar graphs represent the ECL response of the logic gate with the presence of four different input combinations. The dashed red line shows the threshold that separates output 0 and 1. OR logic gate system consisting of  $1 \times 10^{-8}$  M TPrA and  $3.0 \times 10^{-7}$  M Pro as inputs. XOR logic gate system consisting of  $1 \times 10^{-8}$  M TPrA and  $1 \times 10^{-7}$  M DA as inputs. INHIBIT logic gate system consisting of  $1 \times 10^{-8}$  M TPrA and  $1 \times 10^{-4}$  M MB as inputs.

- xiii. **Figure S13.** Schematic illustration of the mechanism for the ECL reaction of the BPEA MWs with TPrA, DA and MB.  $P_{\text{TPrA}}$  is the oxidation product of TPrA and  $P_{\text{DA}}$  is the reduced product of  $\text{DA}^{+}$ .
- xiv. **Figure S14.** ECL kinetic curves of the (A XOR B) INHIBIT C three-input logic gate operations.

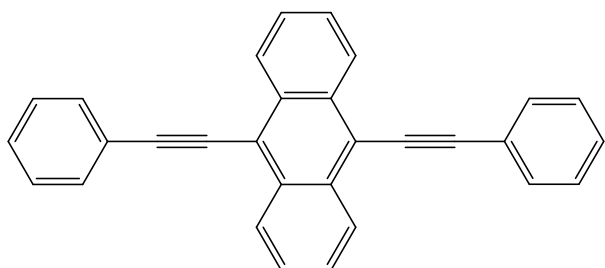


**Figure S1.** Molecular structure of 9,10-bis(phenylethynyl)anthracene (BPEA).

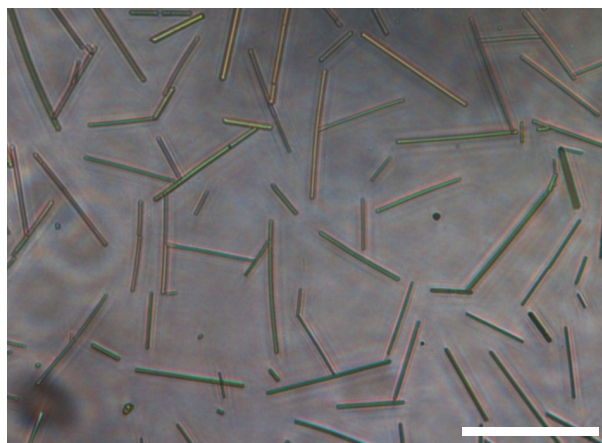


**Figure S2.** The bright-field microscopy image of the BPEA MWs. Scale bar is 30  $\mu\text{m}$ .

The bright-field microscopy image of as-prepared BPEA MWs indicates that the obtained materials have a 1D wire-like structure with length of tens of micrometers.

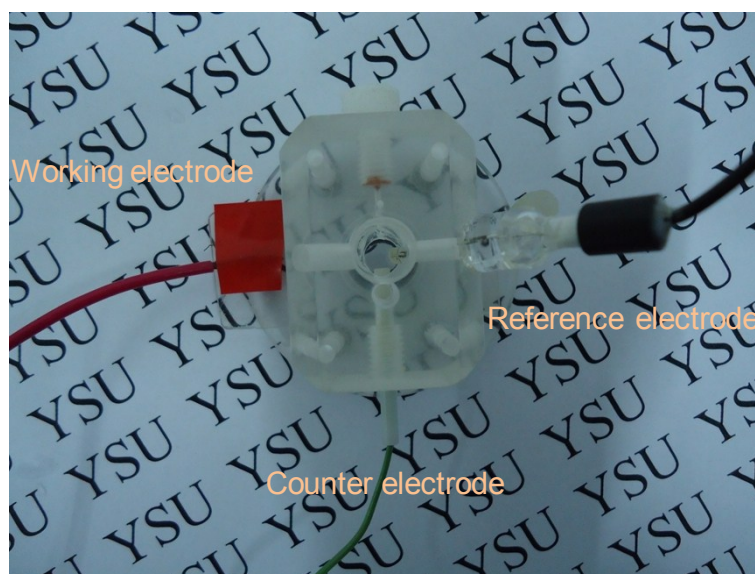


**Figure S3.** The photograph of a typical ECL cell.

A conventional three-electrode system was applied, where the ITO, platinum wire, Ag/AgCl electrode (sat. KCl) was used as the working electrode, counter electrode and reference electrode, respectively.

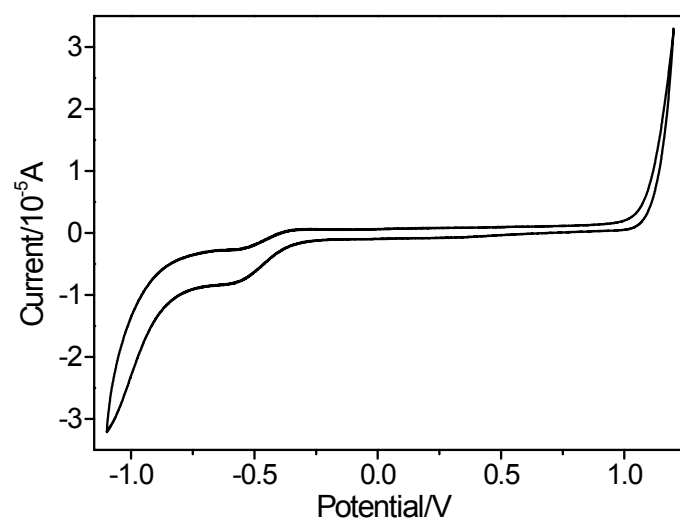


**Figure S4.** The cyclic voltammograms of BPEA MWs/ITO in 0.1 M KCl aqueous solution. Scan rate: 300 mV/s.

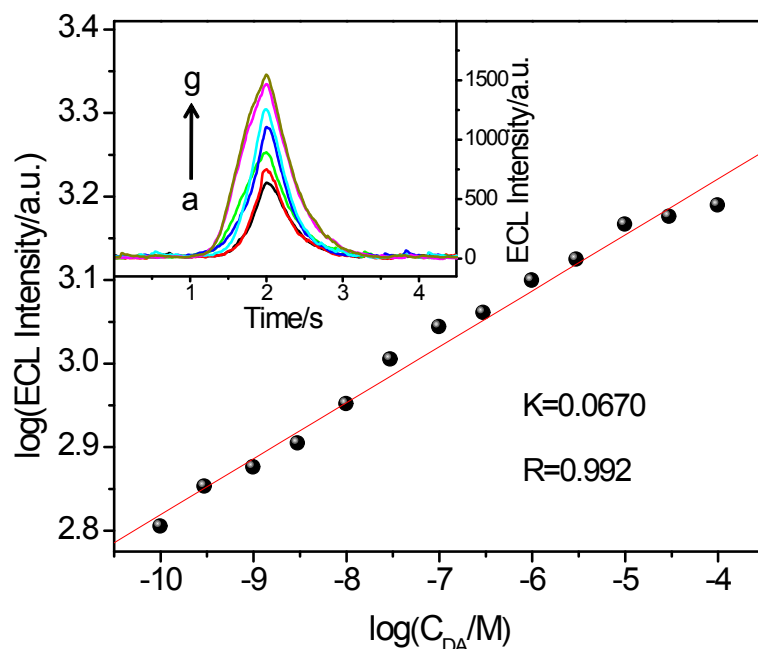


**Figure S5.** Linear calibration plot for the dependence at wide DA concentration of BPEA MWs/ITO ECL system. K is the slope of the line; R is the Pearson product-moment correlation coefficient. Inset: Dependence of the ECL intensity of the BPEA MWs/ITO on the concentration of DA from a to g:  $1.0 \times 10^{-10}$  M,  $1.0 \times 10^{-9}$  M,  $1.0 \times 10^{-8}$  M,  $1.0 \times 10^{-7}$  M,  $1.0 \times 10^{-6}$  M,  $1.0 \times 10^{-5}$  M,  $1.0 \times 10^{-4}$  M. Scan rate: 300 mV/s.

The ECL sensors give the near-linear detection ranges from  $1.0 \times 10^{-10}$  M to  $1.0 \times 10^{-4}$  M towards the determination of the DA. These results indicate that the prepared sensor could be used for the monitoring of trace amounts of DA.



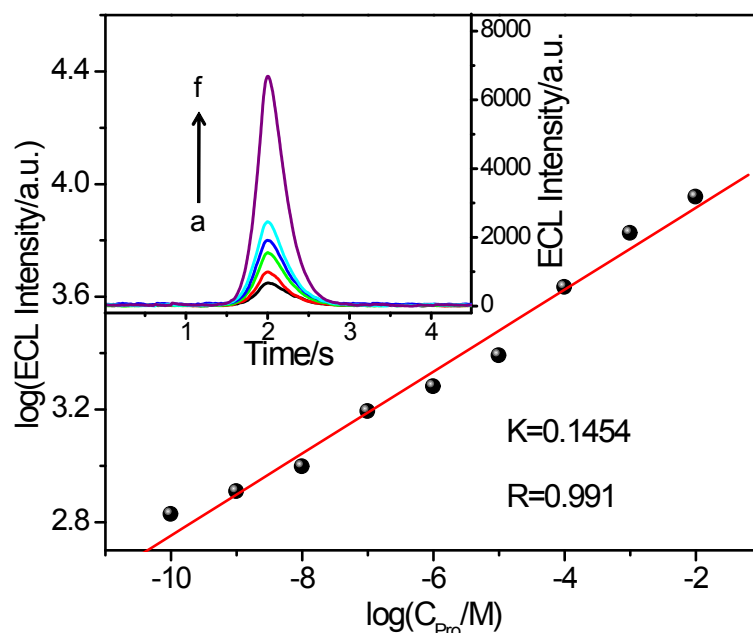


**Figure S6.** Linear calibration plot for the dependence at wide Pro concentration of BPEA MWs/ITO ECL system. K is the slope of the line; R is the Pearson product-moment correlation coefficient. Inset: Dependence of the ECL intensity of the BPEA MWs/ITO on the concentration of Pro from a to f:  $1.0 \times 10^{-10}$  M,  $1.0 \times 10^{-8}$  M,  $1.0 \times 10^{-7}$  M,  $1.0 \times 10^{-6}$  M,  $1.0 \times 10^{-5}$  M,  $1.0 \times 10^{-3}$  M. Scan rate: 300 mV/s.

The ECL sensors give the near-linear detection ranges from  $1.0 \times 10^{-10}$  M to  $1.0 \times 10^{-2}$  M towards the determination of the Pro. These results indicate that the prepared sensor could be used for the monitoring of trace amounts of Pro.

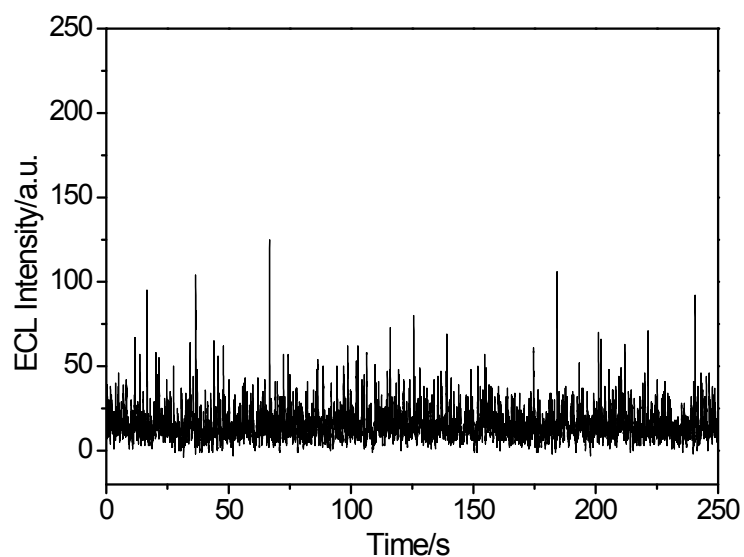


**Figure S7.** ECL emission signal of the BPEA MWs/ITO in 0.1 M KCl aqueous solution containing  $1.0 \times 10^{-5}$  M MB.

No ECL signal can be found when MB was added to the electrolyte, which indicates that the MB cannot be used as co-reactants to take part in ECL reactions with the BPEA MWs.

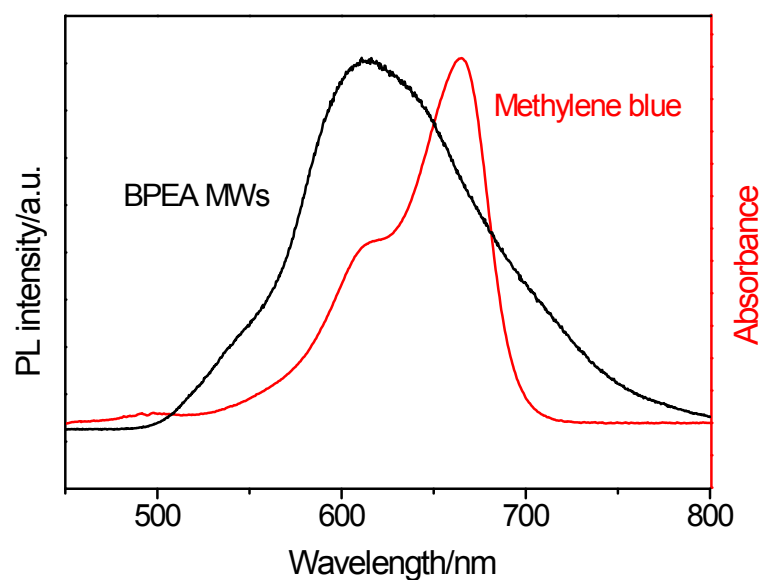


**Figure S8.** Spectral overlap between the PL emission spectrum of BPEA MWs (Black curve) and the absorption spectrum of MB dissolved in H<sub>2</sub>O (Red curve).

The absorption spectrum of MB overlaps well with the BPEA PL spectrum, which indicates that resonance energy transfer from the excited state BPEA\* to MB can occur leading to the decrease of the ECL intensity.

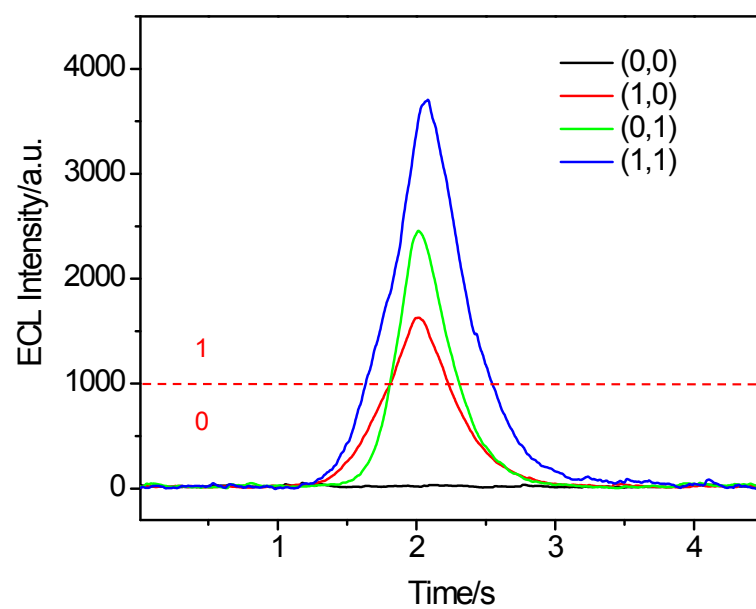


**Figure S9.** ECL kinetic curves of the OR logic gate.

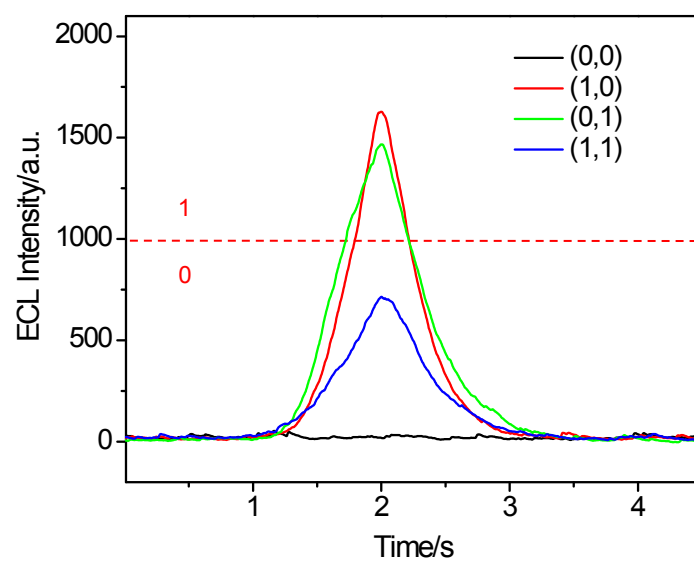


**Figure S10.** ECL kinetic curves of the XOR logic gate.

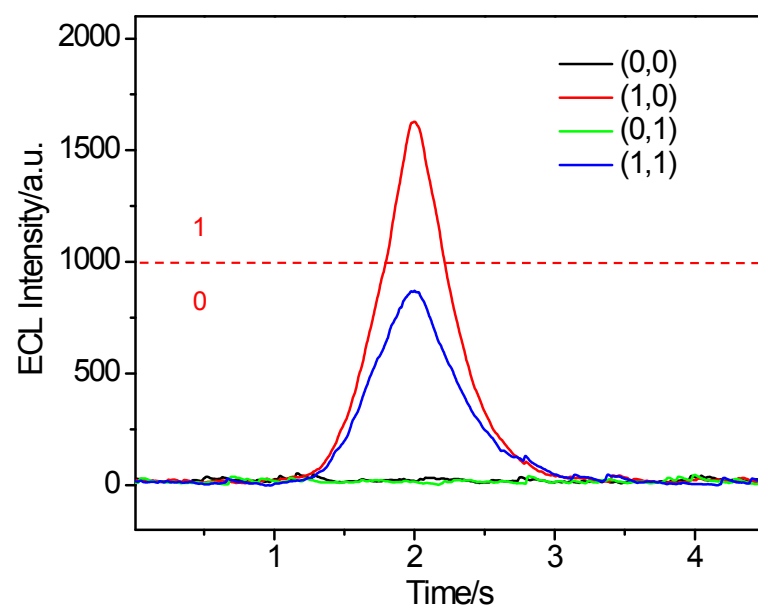


**Figure S11.** ECL kinetic curves of the INHIBIT logic gate.

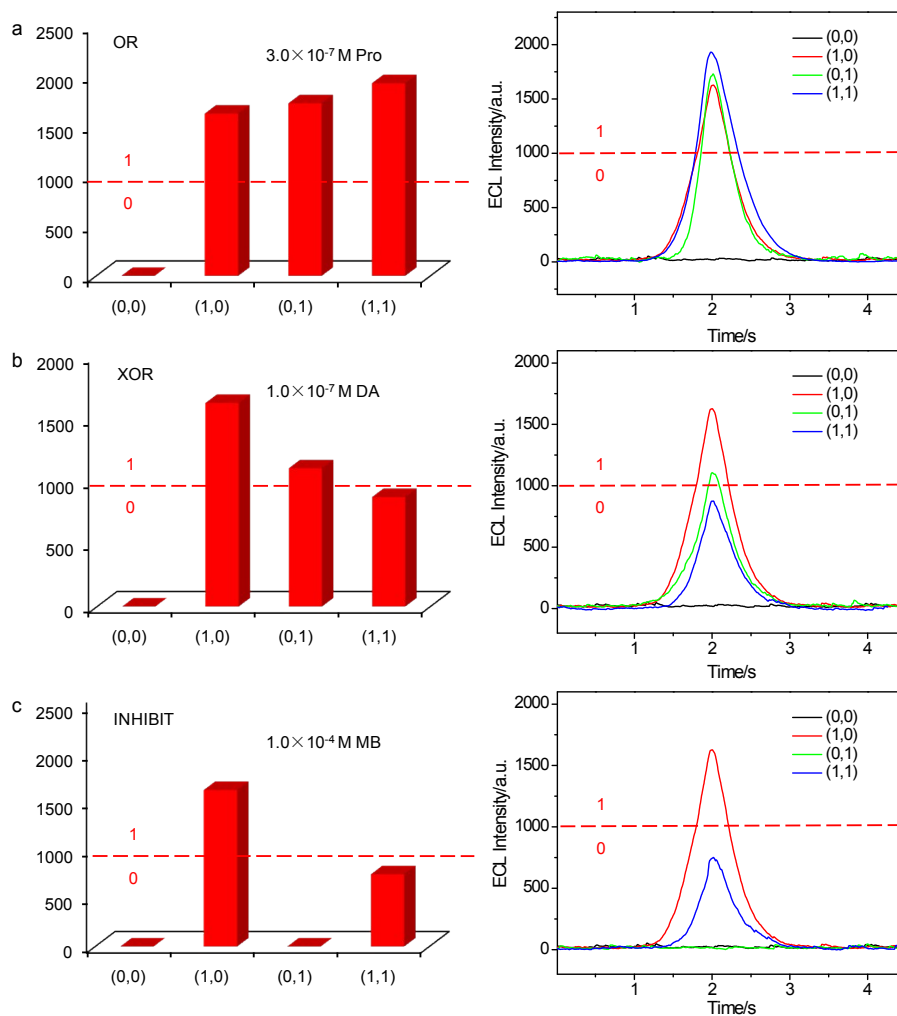


**Figure S12.** Schematic representation of the ECL system which performs the (a) OR, (b) XOR and (c) INHIBIT logic gates under the presence of other concentrations of ECL active molecules. The bar graphs represent the ECL response of the logic gate with the presence of four different input combinations. The dashed red line shows the threshold that separates output 0 and 1. OR logic gate system consisting of  $1 \times 10^{-8}$  M TPrA and  $3.0 \times 10^{-7}$  M Pro as inputs. XOR logic gate system consisting of  $1 \times 10^{-8}$  M TPrA and  $1 \times 10^{-7}$  M DA as inputs. INHIBIT logic gate system consisting of  $1 \times 10^{-8}$  M TPrA and  $1 \times 10^{-4}$  M MB as inputs.

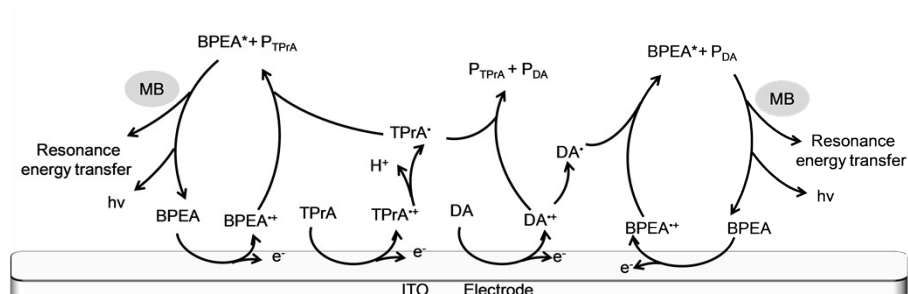


**Figure S13.** Schematic illustration of the mechanism for the ECL reaction of the BPEA MWs with TPrA, DA and MB. P<sub>TPrA</sub> is the oxidation product of TPrA and P<sub>DA</sub> is the reduced product of DA<sup>•+</sup>.



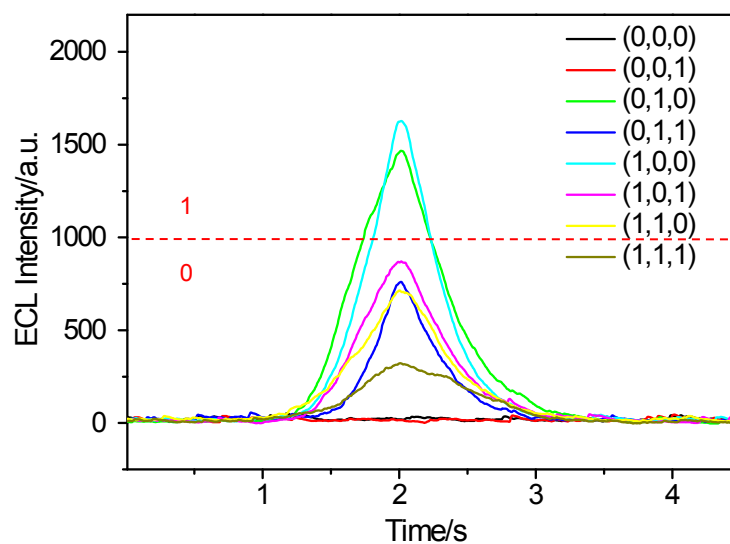


**Figure S14.** ECL kinetic curves of the (A XOR B) INHIBIT C three-input logic gate operations.